Processing of secondary radiation and cosmic ray data measured at flight altitudes with the pixel detector Timepix

María del Carmen Salazar[1]*, **Carlos Granja**[2]

[1]Universidad San Francisco de Quito USFQ, Colegio de Ciencias e Ingeniería, Departamento de Física, Quito, Ecuador

[2]Advacam, Prague, Czech Republic

*Autor para correspondencia / Corresponding Author: mariadelcarmensalazar1980@gmail.com

Tratamiento de los datos de radiación secundaria y rayos cósmicos medidos a altitudes de vuelo con el detector de píxeles Timepix

....

Abstract

Experimental data of the secondary radiation field and cosmic rays inside passenger aircraft in the atmosphere at airline altitudes (10-12 km) were processed. High-resolution data were measured by the semiconductor pixel detector Timepix operated in a miniaturized radiation camera MiniPIX-Timepix. The detector provides precise characterization with quantum sensitivity in terms of deposited energy and visualization of the charged particle radiation and X-ray field. The data were processed at the pre-processing and processing level with an integrated SW tool (Data Processing Engine-DPE). Results and physics data products consist of particle flux, dose rate, deposited energy, deposited dose, field composition into broad particle classes (protons, electrons, X rays), and detailed visualization of the radiation field with quantum imaging registration of single particle tracks. In this work, the detailed analysis of two measurements, as well as comparative graphs of selected results between ten flights, is presented. Results of total absorbed dose are compared with values measured also by Timepix detectors on ground and in LEO orbit onboard a satellite.

Keywords: radiation detection, radiation in the atmosphere, particle tracking, radiation imaging, pixeldetectors, nuclear physics, cosmic rays

Resumen

En este trabajo se procesaron datos experimentales del campo de radiación mixta medidos en el interior de aviones de pasajeros en la atmósfera a altitudes aéreas (10-12 km). Los datos detallados fueron medidos por el detector de píxeles semiconductor Timepix operado en una cámara de radiación miniaturizada MiniPIX-Timepix, el cual proporciona caracterización precisa, sensibilidad cuántica en términos de energía depositada y la visualización de radiación de partículas cargadas. Los datos se procesaron con una herramienta SW integrada (Data Processing Engine-DPE). Los resultados y productos de parámetros físicos consisten en flujo de partículas, tasa de dosis, energía depositada, dosis depositada, composición del campo en amplias clases de partículas

Artículo/Article
Sección A/Section A
Vol. 15, nro. 2
e3127

Processing of secondary radiation and cosmic ray data measured at flight altitudes with the pixel detector Timepix
Salazar / Granja (2023)

(protones, electrones, rayos X), así como la visualización detallada del campo de radiación y registro de imágenes cuánticas de huellas de partículas individuales. En la parte principal de este trabajo se presenta el análisis detallado de dos mediciones, así como gráficos comparativos de resultados seleccionados entre todos los vuelos. Los resultados de la dosis total absorbida se comparan con los valores medidos en tierra y en órbita LEO a bordo de un satélite.

Palabras clave: detección de radiación, radiación en la atmósfera, detectores de pixeles, física nuclear, física de partículas, rastreo de partículas, rayos cósmicos

INTRODUCTION

There are several reasons to study and measure the radiation field in aircraft at flight altitudes [1]. Although we are all exposed to a certain dose of radiation in our daily lives, aircrew members and passengers are subjected to a higher radiation exposure rate than people on the ground under natural conditions [2]. The increase in ionizing radiation with increasing altitude is due to the interaction of galactic cosmic radiation (GCR) with the atmosphere. The composition, intensity, and energy spectra of primary particles are modified by energy loss, nuclear interactions, and secondary particles created [2].

According to the ICRP (International Commission on Radiological Protection) recommendations [3], the exposure of aircrew members to cosmic radiation in jet aircraft may be regarded as occupational exposure, so monitoring the radiation exposure of crew and passengers is not just important, but necessary. It also serves to study the effects of radiation on electronic and avionics components [4], as well as space weather physics in the atmosphere at airline altitudes. These measurements can also play a role in detecting and studying energetic and highly variable solar particle events (SPE) and coronal mass ejections [5].

Semiconductor pixel detector Timepix

The hybrid semiconductor pixel detector Timepix, developed by CERN Medipix Collaboration [6], is a suitable device for accurate in-flight radiation dosimetry [5]. Timepix provides single-quantum sensitivity (photon counting), per-pixel spectrometry, high granularity, noiseless (dark-current free) detection, and particle tracking capability [7]. The detector consists of a radiation-sensitive semiconductor sensor, which is bump-bonded to the pixelated readout ASIC Timepix chip as can be seen in Figure 1. It is equipped with highly integrated signal per-pixel (px) electronics (amplifier, amplitude discriminators, digital counter) [6].

These detectors can use sensors made of different materials (Si, CdTe, GaAs) and thicknesses (100 µm, 300 µm, 500 µm, and 1000 µm for Si). Timepix provides a high-density matrix of 256 × 256 energy- sensitive pixels (total of 65.536 essentially independent pixels) with a pixel pitch of 55 µm and a full sensitive area of 14 mm × 14 mm = 1.98 cm^2 [6].
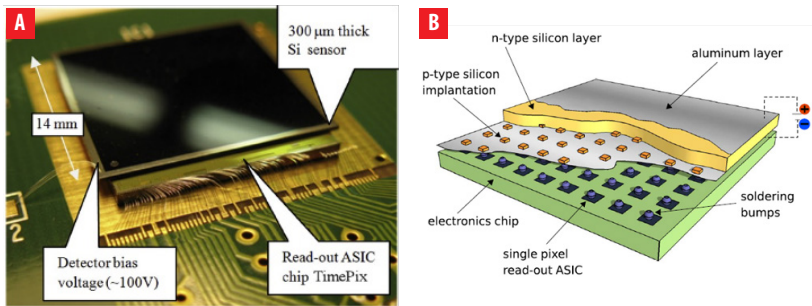
Figure 1. Photo (a) and illustration (b) of the Timepix chip assembly consisting of a semiconductor radiation sensitive sensor (300 μm Silicon, full size 14mm×14mm) bump-bonded to the ASIC Timepix readout chip [8].

Radiation Camera MiniPIX-Timepix

The pixel detector was operated as a compact radiation camera MiniPIX-Timepix which is developed and supplied by Advacam [8]. The MiniPIX is a miniaturized, low-power consumption, single particle counting (or particle tracking) radiation camera (shown in Figure 2) equipped with the semiconductor pixel detector Timepix. The standard MiniPIX system incorporates a single Timepix detector (256 x 256pixels with a pitch of 55 μm) with sensor according to customer preference and standard 300 μm thick silicon as used for this project. The chip-sensor array provides quantum imaging sensitivity for high-resolution spectral tracking of single particles in mixed radiation fields [9]. MiniPIX connects by a single USB 2.0 connector capable of reading up to 45 frames per second (with an exposure time of 1 ms), weighs 25 g, has a power of consumption of 1W, and can be operated at room temperature withoutthe need for active cooling [8]. It is compatible with all major operating systems (MS Windows, Mac OS, and LINUX). The software used to operate the detector, including online response, data readout, andpre-processing, is the PIXET software, also built by Advacam, and can be run on a standard PC.
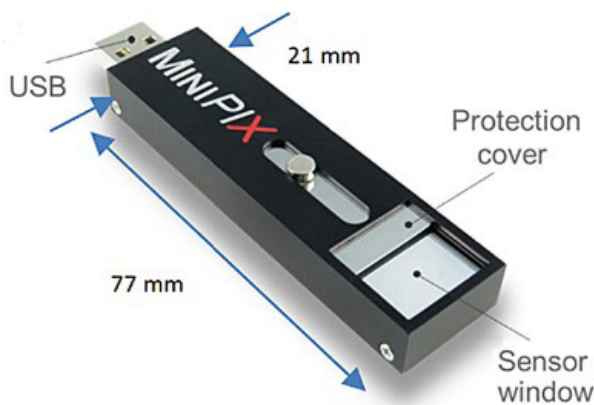

Figure 2. Miniaturized radiation camera MiniPIX-Timepix. Size dimensions 77 mm × 21 mm × 10 mm and connects directly to PC or laptop via single USB connector [5].

Artículo/Article
Sección A/Section A
Vol. 15, nro. 2
e3127

Processing of secondary radiation and cosmic ray data measured at flight altitudes with the pixel detector Timepix
Salazar / Granja (2023)

aci
avances
en ciencias e
ingenierías

METHODOLOGY

The work presented is based on the high-sensitivity detection and precise measurement of radiation in fields such as radiation in the atmosphere, space weather, and cosmic rays. The measurements were performed with the radiation camera MiniPIX-Timepix, in the passenger area of commercial aircrafts at several routes. The Timepix detector was configured to run in *energy (TOT)* mode, which means the deposited energy per pixel is registered.

Quantum-imaging detection of radiation

The hybrid architecture of the Timepix detector provides fast and noiseless (dark-current free) detection of single quanta [6]. It is energy sensitive in terms of deposited energy of low energy charged particles and X-rays. The range of energies that it can detect goes from a few keV (X-rays), tens of keV (electrons), hundreds of keV (protons), and few MeV (ions) [9]. For Silicon sensors, a few tens of keV is the upper range for X-rays and gamma rays, which are detected with limited detection efficiency [9]. For charged particles, Timepix detects all particles, including minimum-ionizing particles such secondary cosmic ray muons and relativistic electrons.

An example of measured data is given in Figure 3, showing the detection and visualization of the radiation field in flight. The single particle tracks are displayed in *quantum-imaging* in either (a) counting mode or in (b) energy mode at the pixel (px) level (black=zero radiation detected, white=radiation detected). The color bar serves as an indicator of deposited energy. All events are registered and processed. Low-energy transfer particles or LCPs such as X-rays and electrons produce small and narrow tracks [5]. High-energy transfer particles or HCPs produce large and broad tracks [9].

A more detailed example of quantum imaging detection and per-pixel scale spectrometry of single particles is shown in Figure 4. Just a small region of the detector matrix is shown for detail and clarity. The data was measured from an ^{241}Am radionuclide source of low-energy gamma rays (which are registered as small tracks of few pixels), X-rays (registered as small tracks of 1 or 2 pixels) and alpha particles (produce large tracks of many pixels) [9].
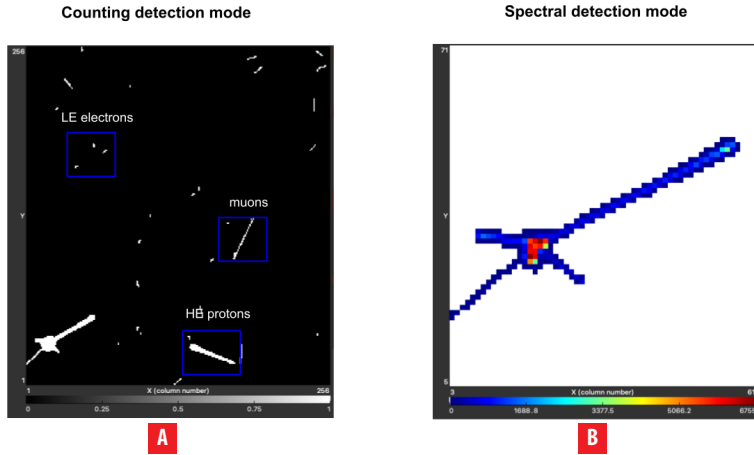
Artículo/Article
Sección A/Section A
Vol. 15, nro. 2
e3127

Processing of secondary radiation and cosmic ray data measured at flight altitudes with the pixel detector Timepix
Salazar / Granja (2023)

Figure 3. Single particles measured by Timepix equipped with a 300 µm Si sensor during flight B described in Table 1. In (a), the visualization of the radiation field observed during a 10- second interval in mid-flight at an altitude of 10 km is given. The entire sensor pixel matrix is shown (256 x 256 pixels = 1.98 cm2). In (b), the detailed detection and visualization of a high Linear Energy Transfer (LET) event is shown. The per-px energy registration is displayed by the color scale in [keV/px]. Only a small region of the detector pixel matrix is displayed (58 x 66 pixels = 0.11 cm2).
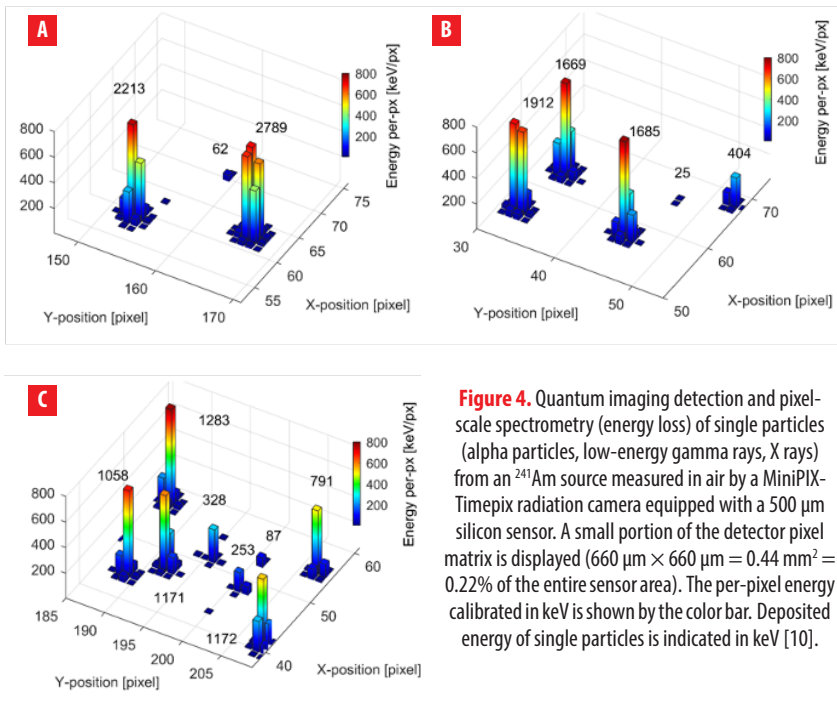

Figure 4. Quantum imaging detection and pixel-scale spectrometry (energy loss) of single particles (alpha particles, low-energy gamma rays, X rays) from an [241]Am source measured in air by a MiniPIX-Timepix radiation camera equipped with a 500 µm silicon sensor. A small portion of the detector pixel matrix is displayed (660 µm × 660 µm = 0.44 mm² = 0.22% of the entire sensor area). The per-pixel energy calibrated in keV is shown by the color bar. Deposited energy of single particles is indicated in keV [10].

Artículo/Article
Sección A/Section A
Vol. 15, nro. 2
e3127

Processing of secondary radiation and cosmic ray data measured at flight altitudes with the pixel detector Timepix
Salazar / Granja (2023)

Measurements

A total of 10 measurements at operational flight altitudes with different routes, dates, and duration wereprocessed. The flights with a duration ≤ 2 hrs were referred to as "short flights," and the other five flights with a duration ≥ 7 hrs were referred to as "long flights," For these measurements, the semiconductor pixel detector Timepix (tpx) and the radiation camera MiniPIX (mpx) were operated in frame mode withan acquisition time of 10 s. The detector was pre-calibrated for per-pixel energy.

The total elapsed time from the start of the measurements until the detector is turned off is the sum of the detector live time + detector dead time (approx 30 ms). The detector's live time is the time intervalin which the data is measured and transferred to the computer system in the dead time. Table 1 shows the measurement results and how the flights were organized.

Table 1. List of data of flights evaluated in this work. SF= short flight. LF=long flight. SN= Detector Serial Number. The frame acquisition time is 10 s. The flight altitudes were between 10 and 12 km.

Label	Date	Route	Route type	Live time [min]	Radiation camera/chip/ SN
A	2022/09/04	PRG-BRUSS	SF	39	mpx/tpx/I10
B	2021/11/10	PRG-MOSCOW	SF	120	mpx/tpx/H09
C	2019/06/30	TOK-WARSAW	LF	401	mpx/tpx/I10
D	2019/06/16	WAR-TOK	SF	75	mpx/tpx/I10
E	2019/06/16	WAR-TOK-NP	LF	620	mpx/tpx/I10
F	2018/12/31	PARIS-TOK	LF	685	mpx/tpx/I10
G	2018/11/10	PRG-DUB.2	LF	815	mpx/tpx/I10
H	2018/11/10	PRG-DUB.3.1	SF	80	mpx/tpx/I10
I	2018/11/10	PRG-DUB.3.2	SF	115	mpx/tpx/I10
J	2018/11/10	PRG-DUB.3.3	LF	653	mpx/tpx/I10

Data Processing

Data processing was performed using the software tool DPE (Data Processing Engine) developed and provided by Advacam. The DPE tool serves for processing of data acquired with the Timepix detectors (tpx, tpx2, tpx3) [11]. The main processing parts of the DPE are:

- **Pre-processing:** Stage for single track clustering, per-px energy calibration is made with detailed event-by-event pattern recognition, and calculation of cluster variables/parameters.

- **Processing:** Production of histograms, particle and radiation field recognition, classification of particle type events.

Artículo/Article
Sección A/Section A
Vol. 15, nro. 2
e3127

Processing of secondary radiation and cosmic ray data measured at flight altitudes with the pixel detector Timepix
Salazar / Granja (2023)

- **Post-processing:** Directional analysis, coincidence analysis, Compton camera, physics product production (particle fluxes, dose rates, deposited energy, LET spectra) and time evolution in relation to radiation field classification.

RESULTS

Detailed results are presented for measurements **B** and **G** described in Table 1.

Detection and visualization of radiation field

Single particles are detected as energy-sensitive tracks called *clusters*. The per-pixel deposited energy is shown in Figures 5 and 6 in the color scale (in keV/px, log scale). The entire detector pixel matrix is displayed, that is, 256 x 256 pixels = 1.98 cm² = 65536 pixels.
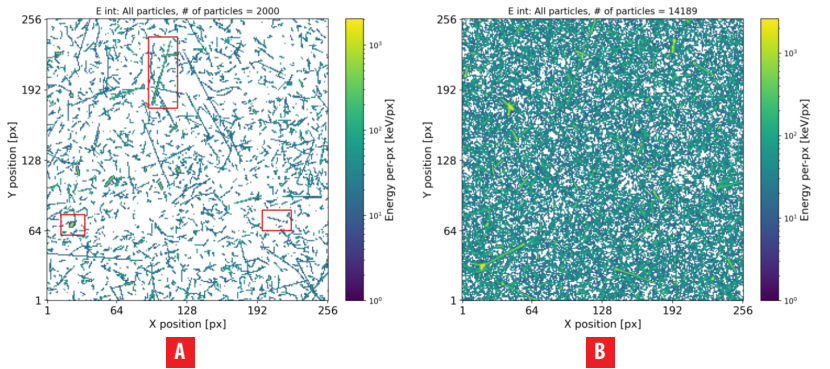

Figure 5. Detection and track visualization of the mixed-radiation field produced during the short flight: B (see Table 1) inside commercial aircraft at operational flight altitudes (10 km). The deposited energy, measured per pixel, is displayed by the color scale. All detected particles are displayed. A total of (a) 2k tracks collected in many frames over 17 minutes where we can see different types of particles (such as those marked in red), and (b) 14189 tracks collected during the whole flight (2 hours) are displayed as a single integrated frame.
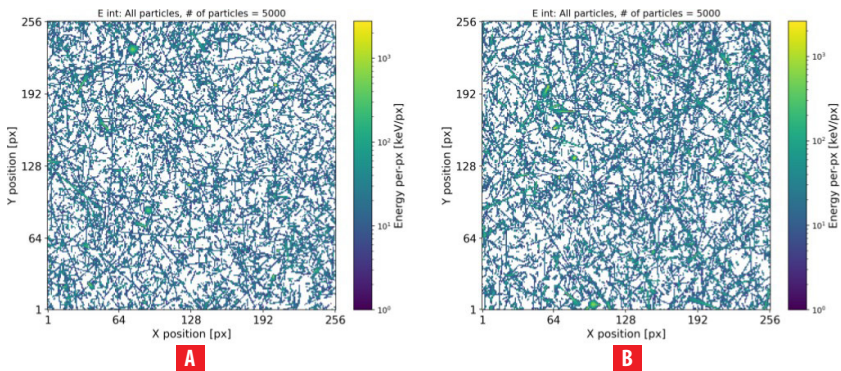

Figure 6. Similar to Figure 5 for data from a long flight: G (see Table 1). Integrated data show 5 k tracks measured in the first 77 min of the flight, and (b) 5 k tracks measured in the last 77 minutes of the flight.

Artículo/Article
Sección A/Section A
Vol. 15, nro. 2
e3127

Processing of secondary radiation and cosmic ray data measured at flight altitudes with the pixel detector Timepix
Salazar / Granja (2023)

aci
avances
en ciencias e
ingenierías

Composition characterization

There is information contained in the morphology and per-pixel spectrometry depending on the particle type, spectra response (energy loss), and direction of incidence to the detector sensor plane [5]. Single particles generate signals in the pixelated semiconductor sensor that involve many pixels forming a cluster of pixels. The charge-sharing effect and the convolution of the deposited charge along its course produce the pattern and morphology of the pixel clusters. High-resolution micro-scale pattern recognition algorithms examine the individual particle tracks with the aim of identifying particle types. [9].

High-energy charged particles traveling in non-perpendicular directions create large tracks with intense energy per pixel. Low-energy charged particles moving perpendicularly to the detector or high-energy particles at perpendicular angles form smaller tracks with minimal per-pixel energy. X-rays generate tiny tracks with few pixels and low energy per pixel. Additionally, interactions involving electrons and gamma rays result in thin, intricate tracks of diverse sizes and shapes, accompanied by low per-pixel energy [5]. Taking this into account, the tracks were filtered into 3 different classes as shown in Table 2.

Table 2. Particle classification into three broad groups according to their energy, direction, and track morphology.

Class	Selected Particles Description
a	Low-energy and/or perpendicular high-let HCPs, namely protons.
b	High-energy and/or non-perpendicular high-let HCPs, namely protons.
c	Low-let LCPs, namely electrons, X rays, gamma rays, muons.

Figures 7 and 8 show the radiation fields seen in Figures 5 and 6 filtered by particle class.
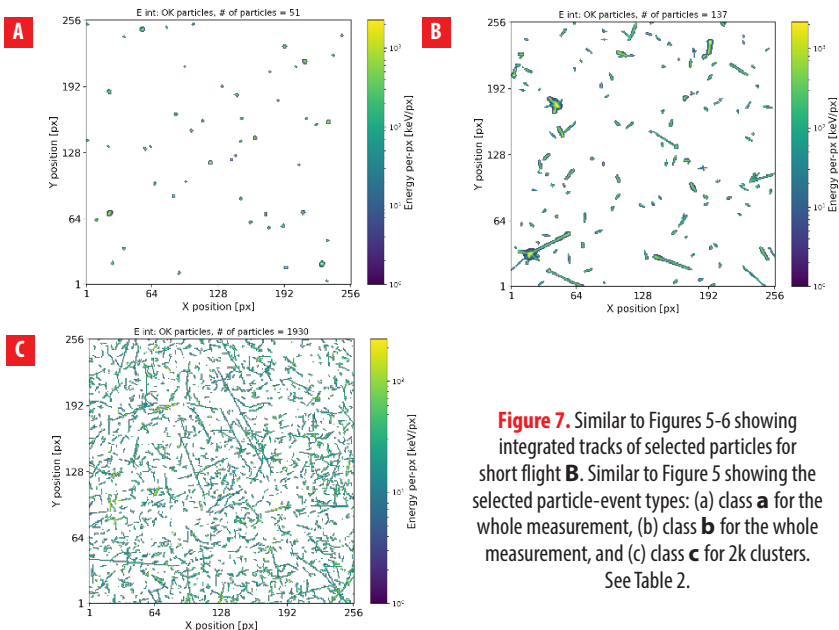
Figure 7. Similar to Figures 5-6 showing integrated tracks of selected particles for short flight **B**. Similar to Figure 5 showing the selected particle-event types: (a) class **a** for the whole measurement, (b) class **b** for the whole measurement, and (c) class **c** for 2k clusters. See Table 2.
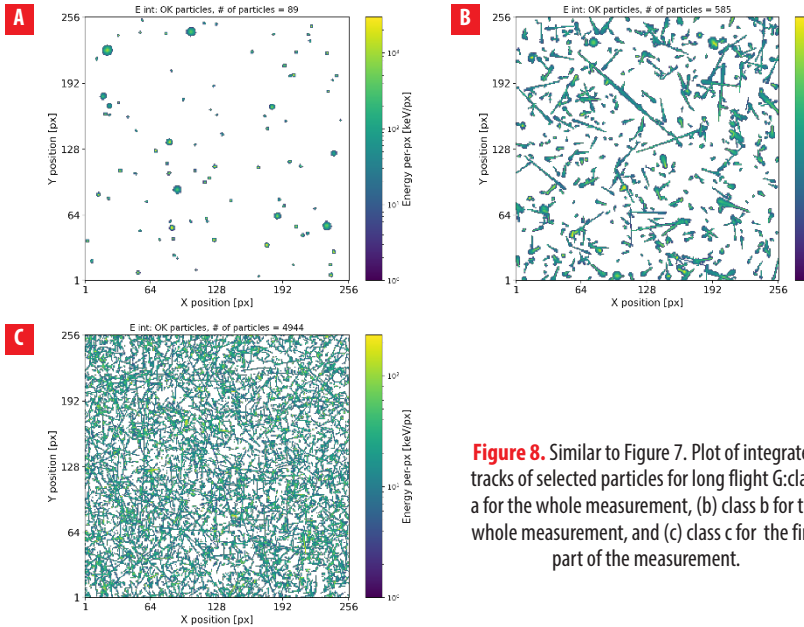
Artículo/Article
Sección A/Section A
Vol. 15, nro. 2
e3127

Processing of secondary radiation and cosmic ray data measured at flight altitudes with the pixel detector Timepix
Salazar / Granja (2023)

Figure 8. Similar to Figure 7. Plot of integrated tracks of selected particles for long flight G:class a for the whole measurement, (b) class b for the whole measurement, and (c) class c for the first part of the measurement.

Event count rates

According to particle class, photons and electrons were the particles detected with highest intensity; heavy charged particles such as protons were detected with lower intensity. Table 3 shows the number of protons, photons, electrons, and light ions (low-energy protons) detected during the sampling time of flights **B** and **G** described in Table 1.

Table 3. Number and percentage of each particle class detected on flights B and G from the Sampling list obtained in the post-processing stage.

Label	Protons		Photons and Electrons		Ions		Total particles	
	(#)	(%)	(#)	(%)	(#)	(%)	(#)	(%)
B	1112	7.8	13068	92.1	9	0.1	14189	100
G	1917	3.7	50488	96.3	36	0.1	52441	100

Particle fluxes

The radiation field can be evaluated in terms of particle flux with particle-type composition sensitivity [5]. The flux of a quantity is defined as the rate at which this quantity passes through a fixed boundary per unit of time. In this case, we are interested in knowing the flux of the different types of particles that have been detected during the flight. The approximate flux can be obtained by normalizing the event count rate to the sensor area (1.98 cm^2) per unit time. Detector efficiencies still need to be taken into

Artículo/Article
Sección A/Section A
Vol. 15, nro. 2
e3127

Processing of secondary radiation and cosmic ray data measured at flight altitudes with the pixel detector Timepix
Salazar / Granja (2023)

account for obtaining real particle flux measurements. Table 4 shows the total particle count, measuredlive time displayed in minutes, and the total flux for each measurement described in Table 1.

Table 4. Total particle count, measured live time, and flux for each measurement.

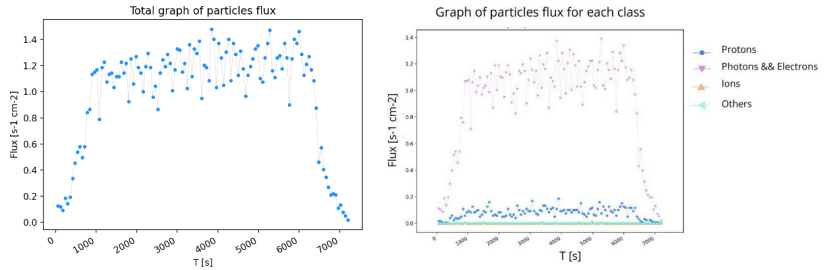| Label	Particles count (#)	Measured live time (min)	Flux (#/min/cm^2)
A	3616	38.94	46.9
B	14189	119.82	59.8
C	47421	400.2	59.7
D	3974	76.09	25.4
E	83752	620.07	68.2
F	86577	685.97	63.7
G	52441	814.78	32.5
H	4728	80.88	29.5
I	9350	113.83	41.5
J	44906	651.82	34.8

Selected flights

Figures 9a and 10a present the particle flux of all types of particles for the two flights previously described, and Figures 9b and 10b show the flux by particle class.
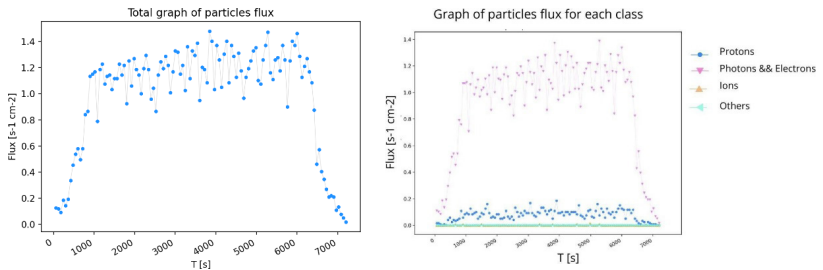
A Particle flux, all particles.　　**B** Particle flux, according to particle class.

Figure 9. Flux for the whole measurement for short flight B.

Artículo/Article
Sección A/Section A

Vol. 15, nro. 2
e3127

Processing of secondary radiation and cosmic ray data measured at flight altitudes with the pixel detector Timepix
Salazar / Granja (2023)

A Particle flux, all particles.

B Particle flux, according to particle class.

Figure 10. Flux for the whole measurement for long flight **G**.

It can be seen that the particle flux increases after the first few minutes of flight. This corresponds to the airplane taking off and gaining altitude, as there are more particles observed than on the ground. The same can be said for the last minutes of the flights; when descending to the ground, the ionizing radiation also decreases. Figure 10b shows an increment in charge particles detected in the last period of the flight. These variations correspond to an increase in flight altitude or changes in the cosmic ray flux over long distances.

Table 5: Particle flux by class of flights **B** and **G** obtained from the Sampling list in the post- processing stage.

Label	Protons flux (#/min/cm²)	Photons and Electrons flux (#/min/cm²)	Ions flux (#/min/cm²)	Total particles flux (#/min/cm²)
B	4.68	55	0.04	59.72
G	1.19	31.25	0.02	32.46

For obtaining the particle fluxes shown in Table 5, the total number of particles detected (by class) is divided by the sampling time in minutes of each flight and for the sensor area.
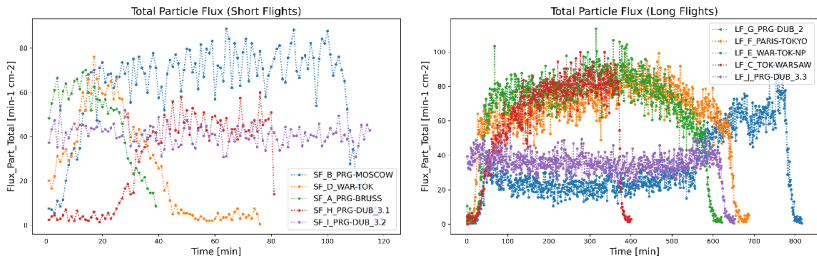
All flights

The particle fluxes of all flights in Table 1 were compared. Plots of the flux of all particles detected and selected particles in short and long flights are presented in Figures 11 and 12.
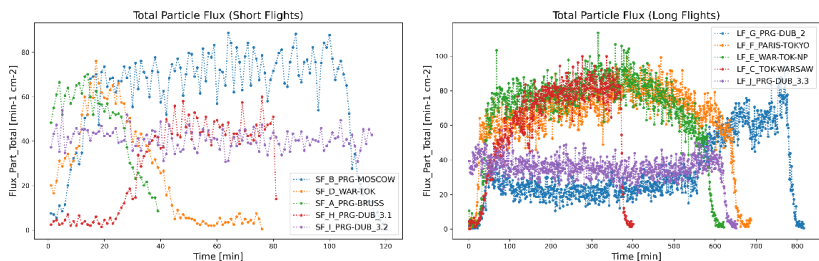
A Particle flux, all particles, short flights: A,B,D,H,I.

B Particle flux, all particles, long flights: C,E,F,G,J.

Figure 11. Particle flux for the whole measurement for all short (left) and long (right) flights described in Table 1.

Artículo/Article
Sección A/Section A

Vol. 15, nro. 2

e3127

Processing of secondary radiation and cosmic ray data measured at flight altitudes with the pixel detector Timepix

Salazar / Granja (2023)

| A | Particle Flux, Photons and Electrons, Short Flights. | B | Particle Flux, Photons and Electrons, Long Flights |

Figure 12. Photons and electrons flux for the whole measurement for all short (left) and long (right) flights described in Table 1.

From Figures 11a and 12a, it can be concluded that the short flight with the highest particle flux and, therefore, the highest radiation was flight **B**; from Figures 11b and 12b, it can be said that the longflights with the highest radiation were flights **E** and **F**, which makes sense since both flights had the samedestination (see Table 1).
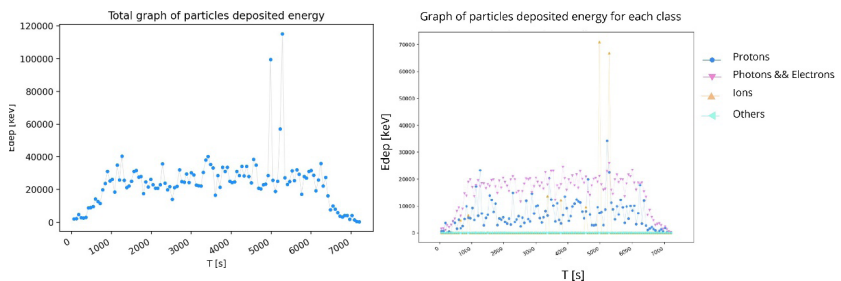
Deposited Energy

The deposited energy (DE) is described as the amount of energy deposited by ionizing radiation in a material per unit mass of the material [12].

Time distribution

Figures 13 and 14 show the deposited energy (measured in keV per time) of the selected flights **B** and **G** described in Table 1. The DE of all particles detected and then separated by particle class is shown. Figures 15, 16, and 17 show the deposited energy of all particles, protons, and photons, respectively, of all short and long flights described in Table 1.

Selected Flights
In Figures 13 and 14, the x-axis, which corresponds to the time in seconds, only takes into account the live time of the detector; it does not include the detector readout dead-time, which is negligible anyway (30 ms in comparison to 10 s, which is the frame acquisition time).

| A | DE, all particles | B | DE, according to particle class |

Figure 13. Deposited energy for the whole measurement for short flight B, measured in keV per second.

Artículo/Article
Sección A/Section A

Vol. 15, nro. 2

e3127

Processing of secondary radiation and cosmic ray data measured at flight altitudes with the pixel detector Timepix

Salazar / Granja (2023)

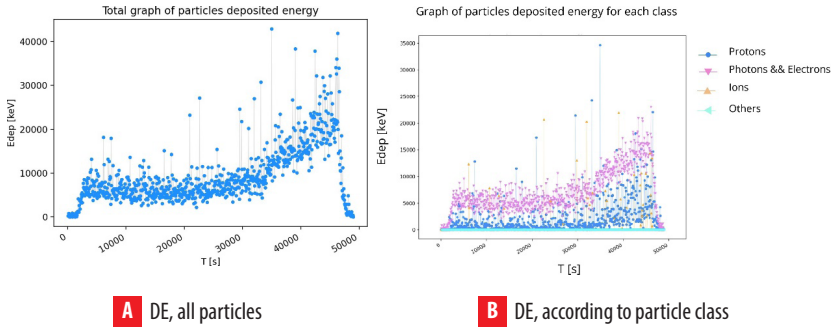| A | DE, all particles |

| B | DE, according to particle class |

Figure 14. Deposited energy for the whole measurement for long flight G, measured in keV per second.

As seen in the previous sections, photons and electrons contribute the highest particle count. However, the presence of protons and ions (HCPs) is notably limited. In Figure 13b and 14b, we can see the distribution of deposited energy depending on the particle type. Despite the relatively low abundance of protons and ions, their cumulative deposited energy constitutes a substantial component of the overall deposited energy (DE). Table 6 shows the average of deposited energy by particle class (protons, photons/electrons, and ions).

Table 6. Deposited energy average in keV by particle class during the sampling time in minutes for measurements B and G described in Table 1.

Label	DE by protons (keV)	DE by photons and electrons (keV)	DE by ions (keV)	Average DE (keV)
B	6935.5	15322.2	1539.8	23797.5
G	2025.6	7069.3	310.56	9405.5

All Flights

Deposited energy plots were generated for all particles and the different particle types, as can be seen in Figures 15, 16 and 17. The measurements were categorized into short flights (SF) and long flights (LF), as detailed in Table 1 for an easier comparison.
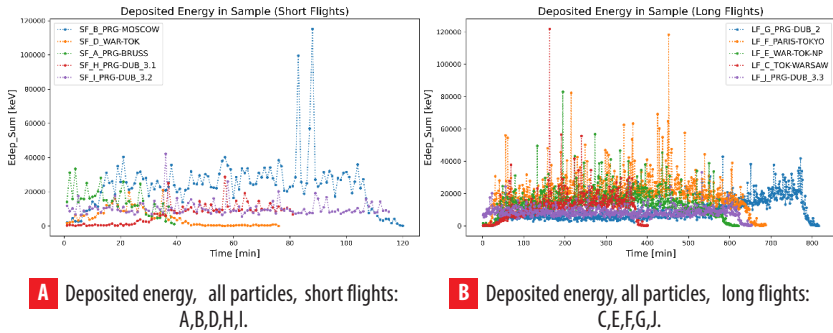
Artículo/Article
Sección A/Section A
Vol. 15, nro. 2
e3127

Processing of secondary radiation and cosmic ray data measured at flight altitudes with the pixel detector Timepix
Salazar / Granja (2023)

A Deposited energy, all particles, short flights: A,B,D,H,I.

B Deposited energy, all particles, long flights: C,E,F,G,J.

Figure 15. Total deposited energy for the whole measurement for all short and long flights described in Table 1, measured in keV per minute.
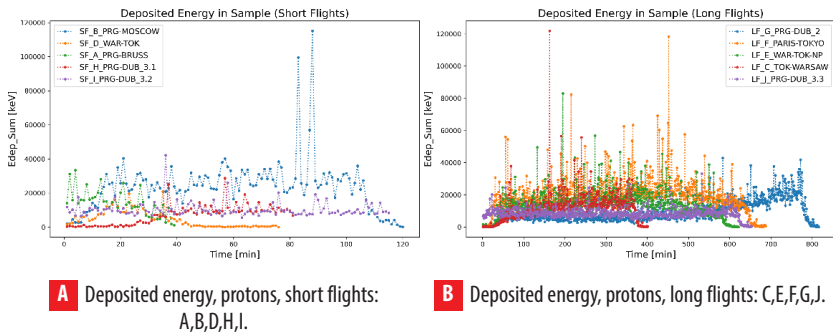

A Deposited energy, protons, short flights: A,B,D,H,I.

B Deposited energy, protons, long flights: C,E,F,G,J.

Figure 16. Deposited energy of protons for the whole measurement for all short and long flights described in Table 1.

A Deposited energy, photons and electrons, short flights: A,B,D,H,I.

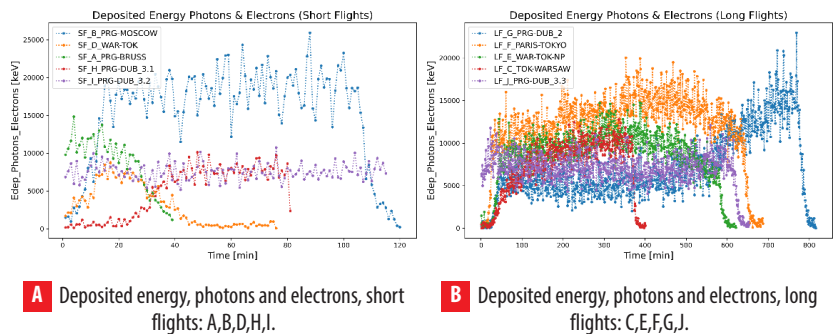**B** Deposited energy, photons and electrons, long flights: C,E,F,G,J.

Figure 17. Deposited energy of photons and electrons for the whole measurement for all short and long flights described in Table 1.

Artículo/Article
Sección A/Section A
Vol. 15, nro. 2
e3127

Processing of secondary radiation and cosmic ray data measured at flight altitudes with the pixel detector Timepix
Salazar / Granja (2023)

It can be observed from Figure 16a and 16b that, although the deposited energy by protons has certain energy peaks, on average, photons and electrons are the particles that deposit the most energy during the flight (See also Figure 17a and 17b). Likewise, according to Figure 15, the short flight with the highest deposited energy was flight **B**, and the long flights with the highest DE were flights **E** and **F**.

Deposited Energy Spectra

The Timepix detector can measure the deposited energy by any particle. In Figure 18 the deposited energy spectra with all particles displayed can be seen. At the top of the following images, a lineal axis is used while a logarithmic axis is used at the bottom.
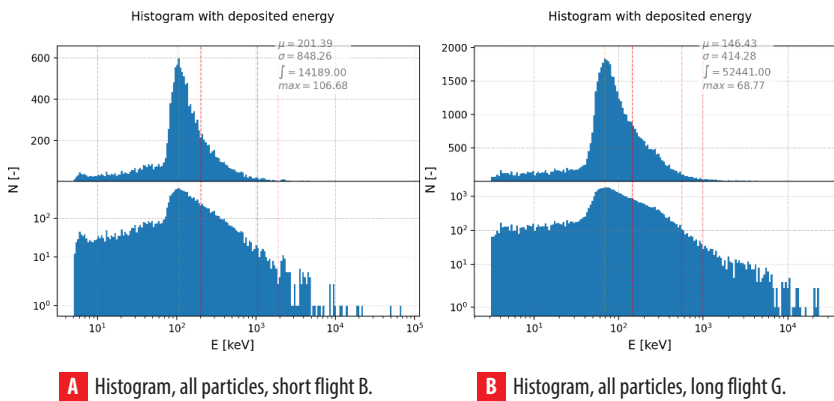
A Histogram, all particles, short flight B.

B Histogram, all particles, long flight G.

Figure 18. Deposited energy spectra of flights B and G described in Table 1.

As can be seen, the deposited energy spectrum is wide, covering ranges from a few keV up to MeV level. The vertical lines shown in Figure 18 will be explained successively from left to right. The yellow vertical line indicates the position of the maximum value. The first red line shows the position of the mean value (μ); the second shows the mean value + standard deviation ($\mu+\sigma$); and the third indicates the mean value + 2 times the standard deviation ($\mu+2\sigma$). The hard part of the spectrum is slightly above 100 keV, which is deposited mostly by protons and HCPs. The soft part of the spectrum, on the other hand, is below 100 keV; this part is produced by LCPs, electrons, X rays, and gamma rays. The energy distribution is quite similar between the two figures, the difference being that less particles were detected in the short flight **B** than in the long one **G**.

Dose rates

The absorbed dose is obtained as the ratio $d\varepsilon/dm$, where $d\varepsilon$ is the average energy deposited by radiation to a material of mass dm:

$$D = \frac{d\varepsilon}{dm}$$

Artículo/Article
Sección A/Section A
Vol. 15, nro. 2
e3127

Processing of secondary radiation and cosmic ray data measured at flight altitudes with the pixel detector Timepix
Salazar / Granja (2023)

The absorbed dose rate (DR) is defined as the rate *dD/dt* where *dD* is the inv crease in absorbed doseduring the time interval *dt*:

$$DR = \frac{dD}{dt}$$

Dose rate is often indicated in micro grays per hour [μ*Gy/h*].

Selected flights

Figures 19 and 20 show the resultant dose rate (μG/h) throughout flights **B** and **G**, described in Table1. The dose rate obtained from all particles is shown in Figures 19a and 20a and then separated by class in Figures 19b and 20b, where it can be seen that photons and electrons are the particles that deposit the highest dose rate followed by protons.
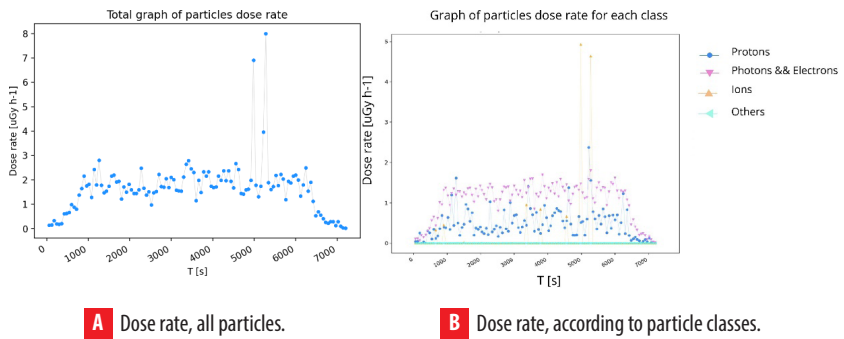

| **A** Dose rate, all particles. | **B** Dose rate, according to particle classes. |

Figure 19. Dose rate for whole measurement for short flight B.

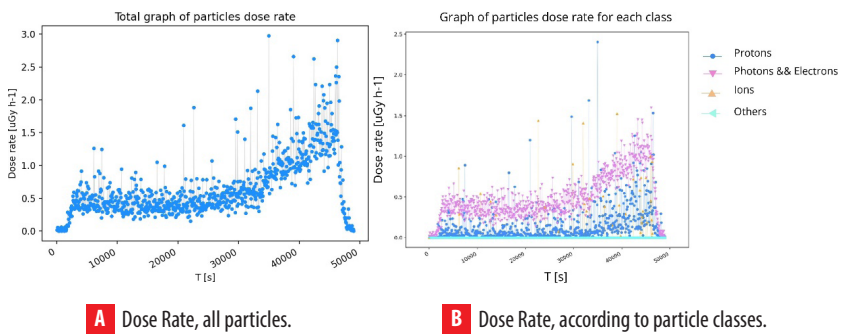| **A** Dose Rate, all particles. | **B** Dose Rate, according to particle classes. |

Figure 20. Dose rate for whole measurement for long flight G.

Generally, the dose rate in the first and last seconds of flight is expected to be low. In Figure 20 we can see a small variation in the last minutes of the flight, which can reflect changes in the flux of cosmic rays over long distances. Fluctuations of small duration, which can significantly increase the dose rate in a short time interval during the flight, also occur.

Artículo/Article
Sección A/Section A
Vol. 15, nro. 2
e3127

Processing of secondary radiation and cosmic ray data measured at flight altitudes with the pixel detector Timepix
Salazar / Granja (2023)

All flights

Figure 21 shows the dose rate of all particles for all flights described in Table 1.

A   Dose Rate, all particles, short flights A,B,D,H,I.   **B**   Dose Rate, all particles, long flights C,E,F,G,J.
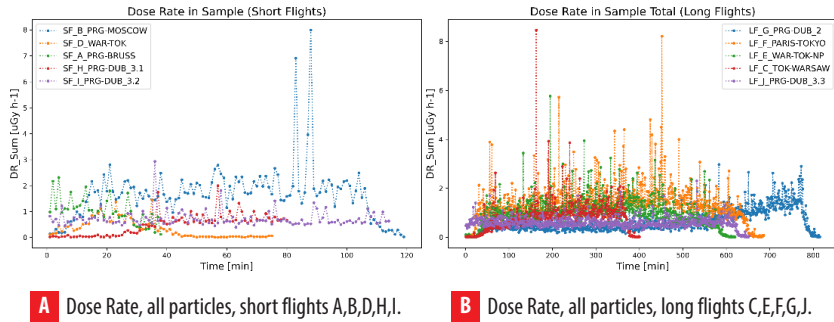
Figure 21. Dose rate for the whole measurement for (a) short and (b) long flights described in Table 1.

In general, the dose rate is low at ground level (at the beginning of the measurement) up to a few km altitude (data taken a few minutes after the plane took off), and then it increases above 3 to 4 km, usually. In long flights, small variations (see blue data in Figure 21b), which can be interpreted as changes in the flux of cosmic rays over long distances, can be seen.
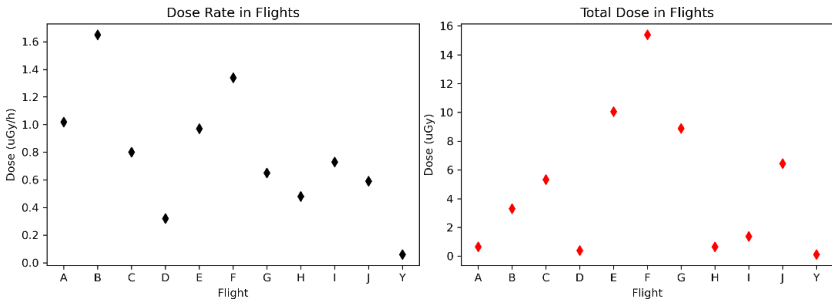
Dose

In contrast to the dose equivalent rate, whose calculation requires knowledge of the quality factor (QF) and LET (as was done in [5]), the total detected dose received during the measurement time can be calculated given the dose rate and the sampling time of each measurement. Table 7 shows the different flights with their detection time in hours, the average dose rate in (μGy/h), the calculated dose given in (μGy), and the standard deviation of each flight data. To compare the measurements as a function of altitude, two new data (Y, Z) have been added. The **Y** label refers to the measurement on the ground (Prague) with the same detector as the previous flights, and the **Z** label is the measurement in LEO orbit onboard Proba-V satellite [13], approximately at 830 km altitude. These data were obtained from Table 1 in [5] and Table 3 in [13], respectively.

Artículo/Article
Sección A/Section A
Vol. 15, nro. 2
e3127

Processing of secondary radiation and cosmic ray data measured at flight altitudes with the pixel detector Timepix
Salazar / Granja (2023)

Table 7. Dose rate, Total Dose, and Standard Deviation during each flight described in Table 1. Y is the ground dose in 2 h at 200 m altitude in Prague. Z is the dose given by the satellite (Proba-V) in 1 h at 820 km altitude.

Label	Time (h)	Average Dose Rate (µGy/h)	Dose (µGy)	Standard Deviation
A	0.65	1.02	0.66	0.53
B	2	1.65	3.3	1.06
C	6.68	0.8	5.33	0.66
D	1.27	0.32	0.4	0.34
E	10.35	0.97	10.06	0.58
F	11.45	1.34	15.39	0.75
G	13.6	0.65	8.88	0.46
H	1.35	0.48	0.65	0.4
I	1.9	0.73	1.38	0.31
J	10.88	0.59	6.44	0.22
Y	2	0.06	0.12	
Z	1	3360	3360	

A Average Dose Rate, all particles, all flights including values on ground (Y).

B Total dose, all particles, all flights including values on ground (Y).

Figure 22. Average dose rate and total dose of all flights during the whole measurement time, which was different for each flight.

We can observe how the ground values (Y) in a 2-hour interval are almost 4 times lower than the lowest dose measured at flight altitudes. On the other hand, the dose given by the satellite in one hour at approximately 820 km altitude is more than 200 times higher than the highest dose measured in flight. It is also important to note how the total dose varies with respect to the dose rate depending on the exposure time. Although Figure 22a shows that **B** flight is the one with the highest dose rate, as being a short flight, its total dose is not as significant as the dose of flight **F**, for example (see Figure 22b).

Artículo/Article
Sección A/Section A
Vol. 15, nro. 2
e3127

Processing of secondary radiation and cosmic ray data measured at flight altitudes with the pixel detector Timepix
Salazar / Granja (2023)

aci
avances
en ciencias e
ingenierías

Linear-energy-transfer spectra

The Linear Energy Transfer (LET) is given by the ratio of the particle deposited energy (E) along its trajectory to the cluster path length (L) [14].

$$LET = \frac{E}{L}$$

(1)

The energy loss and particle LET were determined in the sensor material, in this case Silicon. According to their stopping power, particles can be grouped into low LET events (muons, energetic electrons, and X-rays) and high LET events (protons and heavy charged particles, fragmentation nuclear reactions with nuclei in the sensor volume). The event distributions, so called LET spectra, for all particles is shown in Figure 23.
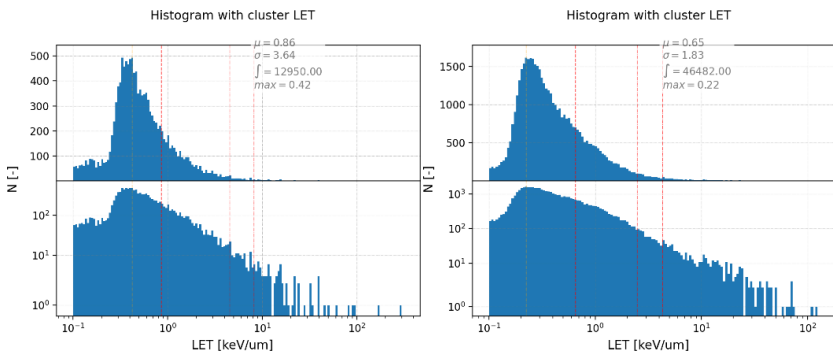
A ALET Histogram for all particles for short flight B.   **B** LET Histogram for all particles for long flight G.

Figure 23. Linear energy transfer distributions.

The results show that most particles exhibit low-LET power, which is below about 1 (keV/μm), a range that corresponds to LCPs (electrons, X and γ rays).

DISCUSSIONS

In this work, a total of 10 operational flight altitude data, measured in the aircraft passenger section, were used. Precise characterization, quantum sensitivity in terms of deposited energy, and visualization of the charged particle radiation and X-ray field were performed by the semiconductor pixel detector Timepix operated in a miniaturized radiation camera MiniPIX-Timepix. Data processing was performed with an integrated SW tool (Data Processing Engine-DPE) provided by Advacam.

From the processed data, information including particle flux, deposited energy, dose rate and the equivalent deposited dose in the sampling time, field composition into broad particle classes (protons, electrons, X-rays), a detailed visualization of the radiation field, and quantum imaging registration of single particle tracks were obtained. To produce

Artículo/Article
Sección A/Section A
Vol. 15, nro. 2
e3127

Processing of secondary radiation and cosmic ray data measured at flight altitudes with the pixel detector Timepix
Salazar / Granja (2023)

the graphs in this article, Python scripts provided by C. Granja, from ADVACAM, as well as original Python scripts were used.

Based on particle flux, particle classification, and event count rates, the observed incidence of events showed a sudden increase just after takeoff, probably due to the aircraft ascending. On the other hand, the decrease in particle count, in the final seconds of the flight, coincides with the descent to ground. For measurement G, a clear increase in the detection of charged particles was observed for a period of approximately 2 hours before landing, which may indicate different flight altitudes or variations in the cosmic ray flux at long periods of flight.

In terms of deposited energy, the results confirmed that photons and electrons made up the majority of the particle counts. Energy distribution graphs for various particle types corroborate this result by showing that although protons and ions showed some sporadic energy peaks, they had a lower average energy deposition compared to photons and electrons. It is important to consider that, despite its scarce presence, the cumulative deposited energy of protons and ions emerged as a significant contributor to the total deposited energy.

The dose outcomes showed higher doses in the time interval after takeoff and before landing. Small variations toward the end of flight G were also evident in the corresponding analysis. We compared the in-flight measurements with those taken on the ground (i.e., C. Granja and S. Pospisil, 2014 [5]) and by Prova satellite (i.e., C. Granja et al., 2016 [13]), from which it became evident that the dose rates during flight altitudes are substantially higher than the corresponding ground values. Furthermore, the satellite's dose rate, measured at an altitude of approximately 820 km, is considerably greater than the maximum dose rate detected during flight.

It should be noted that the total dose fluctuates as a function of exposure time relative to the dose rate. As an example of this, we can see that although flight B presented the highest dose rate among all measurements, having a relatively short flight duration, it resulted in a less significant accumulated dose compared to flights such as F or E, which despite having a lower dose rate, accumulate a substantial total dose due to their long duration.

As future work, an analysis with directional fluxes using the directional information from the detector will be considered.

ACKNOWLEDGMENT

Artículo/Article
Sección A/Section A
Vol. 15, nro. 2
e3127

Processing of secondary radiation and cosmic ray data measured at flight altitudes with the pixel detector Timepix
Salazar / Granja (2023)

AUTHOR CONTRIBUTIONS

C. Granja: Supervised and mentored the project, research administration, methodology design, data acquisition, draft review; M. Salazar: Production of tables and figures, validation and verification of results, data interpretation, writing original draft and editing.

CONFLICTS OF INTEREST

The authors declare no conflict of interest.

Artículo/Article
Sección A/Section A
Vol. 15, nro. 2
e3127

Processing of secondary radiation and cosmic ray data measured at flight altitudes with the pixel detector Timepix
Salazar / Granja (2023)

aci
avances
en ciencias e
ingenierías

REFERENCES

[1]   F. Spurny´ et al. (2007). Monitoring of onboard aircraft exposure to cosmic radiation: May–December 2005. *Advances in Space Research*, *40*(11), 1551–1557. doi: https://doi.org/10.1016/j.asr.2006.10.006

[2]   R. Beaujean et al. (2005). Radiation exposure measurement onboard civil aircraft. *Radiation Protection Dosimetry, 116*, 1-4. doi: https://doi.org/10.1093/rpd/nci095

[3]   1990 Recommendations of the International Commission on Radiological Protection. (1991). *Annals of the ICRP, 21*(1-3), 1–201.

[4]   J.B.L. (2005). Jones et al. Space weather and commercial airlines. *Advances in Space Research, 36*(12), 2258–2267. doi: https://doi.org/10.1016/j.asr.2004.04.017

[5]   C. Granja and S. Pospisil. (2014). Quantum dosimetry and online visualization of X-ray and charged particle radiation in commercial aircraft at operational flight altitudes with the pixel detector Timepix. *Advances in Space Research*, 241–251. doi: https://doi.org/10.1016/j.asr.2014.04.006

[6]   T Poikela et al. (2014). Timepix3: a 65K channel hybrid pixel readout chip with simultaneous ToA/ToT and sparse readout. *Journal of Instrumentation, 9*(5), C05013. doi: https://doi.org/10.1088/1748-0221/9/05/C05013

[7]   C. Granja; C. Oancea et al. (2021). Wide-range tracking and LET-spectra of energetic light and heavy charged particles. *Nuclear Instruments and Methods in Physics Research Section A: Accelerators, Spectrometers, Detectors and Associated Equipment, 988*, 164901. doi: https://doi.org/10.1016/j.nima.2020.164901

[8]   C. Granja; K. Kudela et al. (2018). Directional detection of charged particles and cosmic rays with the miniaturized radiation camera MiniPIX Timepix. *Nuclear Instruments and Methods in Physics Research Section A: Accelerators, Spectrometers, Detectors and Associated Equipment, 911*, 142–152. doi: https://doi.org/10.1016/j.nima.2018.09.140

[9]   C. Granja; J. Jakubek et al. (2018). Resolving power of pixel detector Timepix for wide-range electron, proton and ion detection. *Nuclear Instruments and Methods in Physics Research Section A: Accelerators, Spectrometers, Detectors and Associated Equipment, 908*, 60–71. doi: https://doi.org/10.1016/j.nima.2018.08.014

[10] C. Granja; J. Jakubek; et al. (2022). Spectral and directional sensitive composition characterization of mixed radiation fields with the miniaturized radiation camera MiniPIX Timepix2. *Journal of Instrumentation*. doi: https://doi.org/10.1088/1748-0221/17/11/C11014

[11] ADVACAM. (2023). *DPE.* URL: https://wiki.advacam.cz/index.php/DPE.

[12] J.W. Poston. (2003). *Encyclopedia of Physical Science and Technology*. https://www.sciencedirect.com/referencework/9780122274107/encyclopedia-of-physical-science-and-technology

[13] Carlos Granja et al. (2016). The SATRAM Timepix spacecraft payload in open space on board the Proba-V satellite for wide range radiation monitoring in LEO orbit. *Planetary and Space Science, 125*, 114–129. doi: https://doi.org/10.1016/j.pss.2016.03.009

[14] Carlos Granja et al. (2021). Wide-range tracking and LET-spectra of energetic light and heavy charged particles. *Nuclear Instruments and Methods in Physics Research Section A: Accelerators, Spectrometers, Detectors and Associated Equipment, 988*, 164901. doi: https://doi.org/10.1016/j.nima.2020.164901